Proceedings of IMECE2006
2006 ASME International Mechanical Engineering Congress and Exposition
November 5-10, 2006, Chicago, Illinois, USA

IMECE2006-15505

INFLUENCE OF THE TYPE OF OXIDANT IN THE COMBUSTION OF NATURAL GAS INSIDE AN ALUMINUM MELTING FURNACE

Angela O. Nieckele
Dept. Mechanical Eng, PUC/Rio
22453-900, RJ, RJ, BRAZIL
nieckele@mec.puc-rio.br

Mônica F. Naccache
Dept. Mechanical Eng, PUC/Rio
22453-900, RJ, RJ, BRAZIL
naccache@mec.puc-rio.br

Marcos S. P. Gomes
Dept. Mechanical Eng, PUC/Rio
22453-900, RJ, RJ, BRAZIL
mspgomes@mec.puc-rio.br

Rafael C. Menezes
Dept. Mechanical Eng, PUC/Rio
22453-900, RJ, RJ, BRAZIL
rcezar@mec.puc-rio.br

ABSTRACT

The fuel used as energy source for aluminum melting is of extreme importance for a better performance of the process. However, the type of oxidant can also lead to better performance, leading to a greater preservation of the equipments. Air is more abundant and cheaper, however due to the presence of nitrogen, there is undesirable NOx formation. An alternative is to employ pure oxygen. Although it is more expensive, it can lead to a cleaner and much more efficient combustion process, by significantly altering the combustion aspects inside the furnace, such as the shape of the flame and the distribution of temperature and heat flux. In the present work, numerical simulations were carried out using the commercial package FLUENT, analyzing different cases with pure oxygen and air as the oxidant for the combustion of natural gas. The results showed the possible damages caused by the process if long or too intense and concentrated flames are present.

Key Words: *combustion, industrial furnaces, oxidant*

NOMENCLATURE

A	Pre-exponential Factor
Cp	Specific heat
C	Molar concentration
c_μ	Turbulent Viscosity Coefficient
E	Activation Energy
G	Production of κ
g	Gravity Acceleration
h, h^o	Enthalpy, Formation enthalpy
h_{ci}	Lower heating value
I	Radiant Intensity
k	Thermal conductivity
M	Molecular Weight
m	Mass fraction
n	the number of carbon atoms per molecule
P, p	Modified Total Pressure, Pressure
Pr	Prandtl Number
R	Reaction Rate or Universal Gas Constant
Sc	Schmidt Number
S	Source term
T	Temperature
v	Velocity Vector

Greek Symbols

α	Absorption Coefficient
β	Temperature Exponent
ε	Rate of Dissipation of κ or Total emissivity
φ	Equivalence ratio
γ	Concentration Exponent
κ	Turbulent Kinetic Energy
η	Stoichiometric Coefficient
μ	Absolute Viscosity
ρ	Specific Mass
σ	Stefan Boltzmann Constant

Subscripts

ef	Effective Viscosity
i	Species
j, k, p	Reactant Species, Reaction, Product Species
t	Turbulent

INTRODUCTION

There are several industrial combustion applications which may benefit from the use of oxygen-enriched air or pure oxygen as the oxidizer during the combustion process. The resulting effects are many. Oxygen enrichment increases the flame temperature, promotes oxidation, and can lead to smaller pollutant (NOx) emissions compared with hydrocarbon-air systems, due to the absence of nitrogen.

The formation of nitrogen oxides (NOx) in air-feed combustion systems represents a significant source for this pollutant within the industrial sector. With the increase in the world-wide utilization of fossil fuels, the control of NOx emissions has become an issue of global concern. Additionally, with increasing oil prices, the use of lower quality fuels will worsen the problem. Advances in computational modeling tools and the increased performance of computers have made comprehensive modeling of NOx formation and destruction a valuable tool to provide insights and understanding of the NOx reaction processes in combustion systems. This technology has the potential to enhance the application of various combustion techniques used to reduce NOx emissions from practical combustion systems [1].

Numerical modeling has became an important tool in the design and optimization of industrial equipments and also in the prediction of the emission of pollutants such as CO (carbon monoxide), SOx (sulfur oxides), and NOx. Recently, several numerical studies [2-7] were developed to analyze the combustion process with different fuels, using pure air, oxygen or a mixture of both as the oxidizer. These studies provided detailed descriptions for the temperature, velocity and species concentration fields within various geometries of industrial combustion equipment.

In the work by Frassoldati et al. [2], the attention was focused on a new procedure, based on CFD, for the determination of NOx emissions from combustion processes, which allowed the use of very detailed reaction schemes. The predictions of NOx were obtained by post-processing the flow and temperature fields, as predicted by the CFD model, and lumping together computational cells similar in terms of NOx formation. The resulting macro-cells were assumed to be a network of ideal reactors, which were simulated adopting detailed kinetic mechanisms.

Nieckele et al. [3] described a numerical simulation of the 100% oxy-firing combustion process inside an industrial aluminum re-melting reverb furnace. Three different configurations were analyzed including the comparison between the staged versus non-staged combustion processes. The numerical procedure was based on the finite volume formulation and the $\kappa-\varepsilon$ model of turbulence. The combustion was modeled based on the finite rate models of Arrhenius and Magnussen, and the Discrete Transfer Radiation model was employed for predicting the radiation heat transfer. The numerical predictions allowed for the determination of the flame patterns, species concentration distribution, temperature and velocity fields.

The flow field inside aluminum furnaces with different types of burners and operating conditions was analyzed by Nieckele et al. [3, 4]. Nieckele et al. [5] also investigated the influence of the type of fuel (natural gas and liquid fuel) in the combustion process inside the same furnace.

Numerical and experimental investigation in an industrial aluminum melting furnace with oxygen enriched combustion was also carried out in [6]. The temperature distribution on the refractory walls was verified. The model over estimated the turbulent mixture and, on the other hand, the CO (carbon monoxide) concentrations were under estimated near the burner region, probably because the kinetic effects were neglected. Numerical simulations inside an industrial burner in an aluminum melting furnace were also carried out in [7]. It was shown that the flame height grows with the fuel velocity for a given air-fuel ratio, and with the reduction of the air velocity, for a given fuel velocity. In [8] a turbulent natural gas flame in a cylindrical furnace was simulated, using finite rate models and modeling chemical reactions in two different ways: in a simple manner, where the fuel combustion was predicted in one single global reaction; and with a two-step process, where the carbon monoxide could be predicted in an intermediate reaction. The results for both models showed a good agreement with the experimental data found in the literature, although it was observed that the physical phenomena was better described by the two step reaction.

In the present work, numerical simulations were carried out using the commercial package FLUENT, version 6.2 [9], to determine the flow field, species and temperature distribution inside an aluminum industrial furnace, employing air and pure oxygen for the combustion of natural gas. The advantages and disadvantages of each type of oxidant are addressed.

PROBLEM SET-UP

The furnace geometry was represented as a rectangular cube of 4.0 m length, 1.5 m width and 2.0 m height, as presented in Fig. 1, which is an approximation of existing aluminum furnaces. Figure 2 illustrates details of the frontal plane, and different view of the inlet configuration. Due to symmetry, only half furnace was solved.

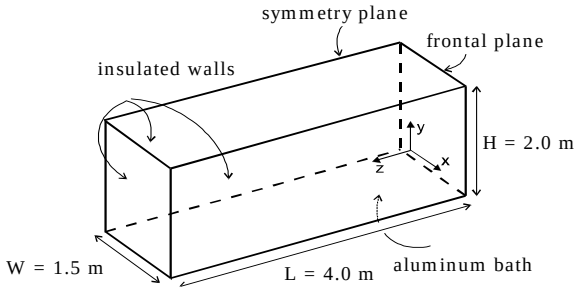

Fig. 1: Schematic of the furnace and geometry.

The lower limit of the furnace was considered to be the liquid aluminum surface with a small aluminum oxide layer of

0.5 mm above it. The aluminum oxide layer was considered to describe the oxidization of the aluminum surface by the water that results from the combustion, which can act as an isolator and can compromise the quality of the product.

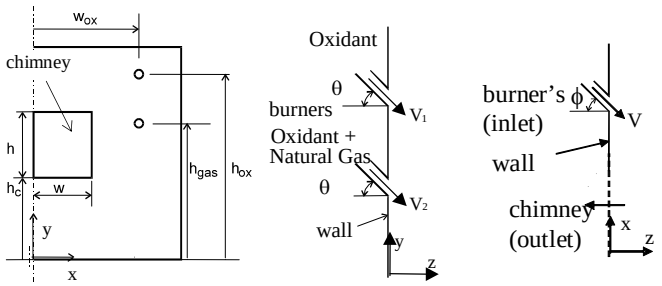

Fig. 2: Injection and chimney geometry.

The vertical symmetry plane passes through the center of the chimney between the two pairs of oxidant and fuel injectors. The inlets of oxidant and fuel as well as the outlet of the combustion products are located at the same wall (Fig. 2). The center of the burner is located 0.65m above the aluminum oxide layer and 0.80m away from the symmetry plane. Fuel is injected in the center and the oxidant surrounds it. The oxidant injector is located 0.20m above the burner. Both burner and oxidant lance are formed by a central opening and a set of small orifices surrounding the central opening, which are represented here by an annular opening. Two cases were analyzed, both with natural gas as fuel, one with oxygen as oxidant and the other with air as oxidant. The inlet geometry of oxidant depends on the oxidant. The natural gas burner has a central opening area equal to 2.89×10^{-4} m^2 for both cases. For the case with oxygen as oxidant, the oxidant and burner lances have the same geometry, and the annular opening area is equal to 1.38×10^{-3} m^2. For the case with air as oxidant, a larger mass flow rate is necessary. Therefore, the inlet areas are larger to maintain the same order of magnitude of the velocity at the entrance. In this case, in the oxidant lance the central opening area is equal to 2.13×10^{-3} m^2. The annular opening areas for both lances are equal to 3.53×10^{-3} m^2. The jets are directed away from the refractory walls, angles of 15° in the vertical plane and 10° in the horizontal plane were set. The height of the center of the rectangular chimney coincides with that for center of the burner, its half width measures 0.50m and its height measures 0.60m.

Considering a typical aluminum load of 16 tons (which corresponds to a volume of 6 m^3), assuming an approximate process time of 1 hour, and knowing that the aluminum latent heat is 397.4 kJ/kg, a heat transfer rate of 880 kW must be extracted from the aluminum surface, in order to represent the energy necessary to melt the entire load of aluminum.

The composition of a typical natural gas can be found in Table 1, where the molecular weight M, formation enthalpy h^o and the specific heat at constant pressure Cp are indicated [10]. The oxygen and air properties and inlet mass concentration are also presented in Table 1.

The absolute viscosity of natural gas was set as $\mu= 1.72 \times 10^{-5}$ Pa s, while the thermal conductivity was taken as k = 0.0241 W/(m K). The diffusion coefficient of all species in all mixtures was equal to the N_2 diffusion coefficient, 2.88×10^{-5} m^2/s. The mixtures specific heats were obtained by a weighted mass fraction average.

The emissivity was set as 0.65 at all refractory walls and equal to 0.8 at the aluminum oxide surface.

	Species	% m_i	M_i	h_i^o kJ/kg	Cp_i J/(kg K)
Natural Gas	CH_4	70.3	16	-74 895	2 222
	C_2H_6	17.8	30	-83 863	1 731
	C_3H_8	0.69	44	-103 860	1 549
	CO	0.00	28	-110 530	1 043
	CO_2	6.93	44	-39 353	840
	N_2	4.28	28	0.0	1 041
Oxygen	O_2	100	32	0.0	919
Air	O_2	23	32	0.0	919
	N_2	77	28	0.0	1 041

Tab. 1: Species properties

MATHEMATICAL MODELING

The turbulent flow and heat transfer inside the furnace were solved numerically using the finite volume technique and the commercial code FLUENT, version 6.2.

The average forms of the conservation equations of mass and momentum are given by:

$$\mathbf{div}\,(\rho \mathbf{v}) = 0 \qquad (1)$$

$$\mathrm{div}(\rho \mathbf{v}\mathbf{v}) = \mathrm{div}[\mu_{ef}\ (\mathrm{grad}\ \mathbf{v} + (\mathrm{grad}\,\mathbf{v})^T] - \mathrm{grad}\ P \qquad (2)$$

where ρ is the density, **v** is the velocity vector, and $\mu_{ef} = \mu+\mu_t$ is the effective viscosity, obtained by the Boussinesq's hypothesis. The modified total pressure $P = p - (2/3)\,[\,\mu_{ef}\,\mathbf{div}\,\mathbf{v} + \rho\,\kappa\,]$, takes into account the contributions due to the turbulent fluctuations.

The turbulence κ–ε model was used for calculating the turbulent viscosity, which is defined as $\mu_t = c_\mu \rho\, \kappa^2/\varepsilon$, where κ is the turbulent kinetic energy and ε the dissipation for the turbulence kinetic energy . The conservation equations of κ and ε are given by:

$$\mathbf{div}\,(\rho \mathbf{v}\kappa) = \mathbf{div}\left[(\mu + \mu_t / \mathrm{Pr}_\kappa)\,\mathbf{grad}\ \kappa\right] + (G - \rho\varepsilon) \qquad (3)$$

$$\mathbf{div}\,(\rho \mathbf{v}\varepsilon) = \mathbf{div}\left[\ (\mu + \frac{\mu_t}{\mathrm{Pr}_\varepsilon})\,\mathbf{grad}\ \varepsilon\ \right] + (c_1 G - c_2 \rho\varepsilon)\ \frac{\varepsilon}{\kappa} \qquad (4)$$

In the Eqs. (3) and (4), Pr_κ and Pr_ε are the turbulent Prandtl numbers for κ and ε, and were set equal to 0.7. The constants were set as c_1=1.4, c_2=1.9, and c_μ=0.09. The term $G = \mu_t\,[\mathbf{grad}\ \mathbf{v} + (\mathbf{grad}\,\mathbf{v})^T]$ o **grad v** stands for the generation of turbulence kinetic energy.

The above equations were solved simultaneously with the conservation equations of mass and momentum, providing the solution for the turbulent flow problem.

The density of the gaseous mixture was calculated using the ideal gas law, $\rho = p_{op} / [RT \Sigma_i (m_i/M_i)]$, where p_{op} is the average operation pressure inside the furnace, that was to be equal to one atmosphere.

For all dependent variables wall functions were employed for setting up the conditions close to the solid boundaries, following the procedure described in [11] and [12].

The temperature field within the furnace was obtained by solving the energy equation, which for Lewis number Le=Pr/Sc = 1 can be written as:

$$\mathbf{div}(\rho\,\mathbf{v}\,h) = \mathbf{div}\left[\left(\frac{\mu}{Pr} + \frac{\mu_t}{Pr_t}\right)\mathbf{grad}\,h\right] + S_h \qquad (5)$$

where the total enthalpy h is defined by the sum of the enthalpies for each species h_i weighted by its mass fraction m_i,

$$h = \Sigma_i\, m_i\, h_i \quad ; \quad h_i = \int_{T_{ref,j}}^{T} Cp_j\, dT + h_j^o(T_{ref,j}) . \qquad (6)$$

and h_i^o is the formation enthalpy at the reference temperature $T_{ref,j}$ and Cp_j is the specific heat at constant pressure of specie j. The term $S_h = S_{reac}+S_{rad}$, represents the enthalpy source due to the chemical reactions (combustion) and the radiation heat transfer. The turbulent Prandtl number, Pr_t, was set at 0.5.

Radiation Model

The source term in the energy equation due to radiation was calculated using the Discrete Transfer Radiation Model (DTRM). In this model, the change in the radiant intensity I, integrated over all wavelengths, along a path S is calculated according to $dI/dS = - \alpha I + \alpha \sigma T^4/\pi$, since scattering is neglected. The terms on the left side represent the loss by absorption and the gain by emission due to the participating medium, respectively.

The model integrates the above expression along several directions starting from each control volume on the domain surfaces. The source term S_{rad} is calculated locally by summing the changes in intensity for all the rays crossing the control volume. The Weighted Sum of Gray Gases Model (WSGGM) was used for the calculation of the absorption coefficient [13].

Chemical Species and Combustion Modeling

The generalized finite rate model, combined with the Arrhenius-Magnussen model [9-10], was selected to obtain the source term due to chemical reactions in the energy equation. The chemical species distributions are obtained through the solution of n-1 transport conservation equations, where n represents the number of species. The general form of the conservation equation for each chemical species is given by

$$\mathbf{div}(\rho\,\mathbf{v}\,m_i) = \mathbf{div}\left[(\mu/Sc + \mu_t/Sc_t)\mathbf{grad}\,m_i\right] + R_i + S_i \qquad (7)$$

In the above equation, the terms R_i and S_i represent the sources for each species. The former is associated with the transformations due to chemical reactions, and the later may represent addition from the dispersed phase. The term R_i , may be expressed by the sum of the reaction rates (generation or consumption) for species i in every reaction k, as denoted by $R_{i,k}$, according to $R_i = \Sigma_k R_{i,k}$. The turbulent effect is taken in consideration by the turbulent diffusion coefficient, μ_t/Sc_t, where the turbulent Schmidt number Sc_t was set equal to 0.5.

With the combined Arrhenius-Magnussen model, the combustion reactions rates are determined by the smallest value between the Arrhenius and the Magnussen models, which are respectively given by

$$R_{i,k} = \eta_{i,k} M_i T^{\beta_k} A_k \exp(-E_k/RT) \prod_j C_j^{\gamma_{j,k}} \qquad (8)$$

$$R_{i,k} = \eta_{i,k} M_i K_1 \rho \frac{\varepsilon}{k}\,\mathbf{min}\left[\frac{m_{j*}}{\eta_{j*,k} M_{j*}}; K_2 \frac{\Sigma_p m_p}{\Sigma_p \eta_{p,k} M_p}\right] \qquad (9)$$

In these expressions j* represents the reactant which gives the smallest value for $R_{i,k}$, and K_1 and K_2 are empirical constants, set as 4.0 and 0.5, respectively [14].

Reactions

Two cases were considered, in the first one, pure oxygen was employed as oxidant while for the second case, air was used as oxidant. For both cases, natural gas was employed as fuel. A four step mechanism was selected, as shown in Table 2.

The stoichiometric coefficients for each reaction must be specified in accordance to equations in Table 2. The Magnussen reaction rate expression does not require any additional information. The parameters for Arrhenius and Arrhenius-Magnussen models [9] are shown in Table 3, where β_k was set as zero for all reactions. The unit of A_k is $(m^3/s)/kmol$ and for E_k is MJ/kmol.

Reaction	
1	$CH_4 + 3/2\ O_2 \rightarrow CO + 2\ H_2O$
2	$CO + 1/2\ O_2 \rightarrow CO_2$
3	$C_2H_6 + 7/2\ O_2 \rightarrow 2\ CO_2 + 3\ H_2O$
4	$C_3H_8 + 7/2\ O_2 \rightarrow 3\ CO + 4\ H_2O$

Tab. 2: Reactions

Reac	A_k	E_k	γ_{CH4}	γ_{C2H6}	γ_{C3H8}	γ_{O2}	γ_{CO2}	γ_{CO}	γ_{H2O}
1	5.01×10^{11}	200	0.7	-	-	0.8	-	0	0
2	2.24×10^{12}	170	-	-	-	0.25	0	1	-
3	6.19×10^{9}	126	-	0.1	-	1.65	0	-	0
4	5.62×10^{9}	126	-	-	0.1	1.65	-	0	0

Tab. 3: Parameters for each reaction for the Arrhenius reaction rate expression, Eq. (9)

NOx prediction

The NOx concentration is predicted using FLUENT NOx postprocessor [9]. Since NOx reaction rates are slow, they are not treated using an equilibrium assumption, as it was performed with the others intermediate and product species. The NOx species can be excluded from the equilibrium calculation because they are present in low concentrations and have little impact on density, temperature and other species concentration.

The NOx emissions are predicted by solving a transport equation for nitric oxide (NO) concentration, using a given flow, temperature and species field. In this work only the thermal [15-16] and prompt [17] mechanisms for NOx formation were considered. Therefore, only the NO species transport equation has to be solved:

$$\mathbf{div}\left(\rho\,\mathbf{v}\,m_{NO}\right)=\mathbf{div}\left(\rho\,D\,\mathbf{grad}\;m_{NO}\right)+S_{NO} \tag{10}$$

The source term S_{NO} is given by:

$$S_{NO}=M_{w,NO}\frac{d[NO]}{dt} \tag{11}$$

where $M_{w,NO}$ is the molecular weight of NO (kg/gmol), and d[NO]/dt is the NO formation rate for each case [9].

Thermal NOx formation is calculated by using the extended Zeldovich mechanism, developed by Zeldovich in 1946 and described in Tomeczek and Gradon [15]. The reaction rates were obtained from the evaluation of Hanson and Salimian [16]. For thermal NOx mechanism the principal reactions employed were:

$$\text{reaction 1: } O+N_2\leftrightarrow N+NO \quad \text{reaction 2: } N+O_2\leftrightarrow O+NO \tag{12}$$

The OH reaction was neglected, once the reaction is not fuel enriched.

Assuming a quasi-steady state for [N], the NO formation rate is given by:

$$\frac{d[NO]}{dt}=2\,k_{f,1}[O][N_2]\frac{\left(1-\dfrac{k_{r,1}\,k_{r,2}\,[NO]^2}{k_{f,1}[N_2]\,k_{f,2}[O_2]}\right)}{\left(1+\dfrac{k_{r,1}[NO]}{k_{f,2}[O_2]}\right)} \tag{13}$$

where [O], [NO], [O2], and [N2] are the concentration of [i] atoms, and $k_{i,j}$ are empirical constants [16], given by:

$$\begin{aligned} k_{f,1}&=1.8\times10^{8}e^{-38370/T} & k_{f,2}&=1.8\times10^{4}e^{-4680/T}\\ k_{r,1}&=3.8\times10^{7}e^{-425/T} & k_{r,2}&=3.81\times10^{3}Te^{-20820/T}\end{aligned} \tag{14}$$

The first subscript of $k_{i,j}$ indicates the reaction direction (f = forward and r= reverse) and the second indicates the reaction of Eq. (12).

The concentration of the oxygen-atom is given by:

$$[O]=3.97\times10^{5}T^{-1/2}[O_2]^{1/2}e^{-31090/T}\quad \text{gmol/m}^3 \tag{15}$$

The presence of a second mechanism for creating NO during the combustion process was first identified by Fenimore [17] and was denominated by "prompt NO". The prompt NO mechanism is more important in rich flames. In the present NOx prompt model, it was used a global kinetic parameter and a procedure developed by De Soete [18]. For the prompt NOx mechanism, the reactions are:

$$\begin{aligned} &CH+N_2\leftrightarrow HCN+N\\ &N+O_2\leftrightarrow NO+O\end{aligned} \quad ; \quad \begin{aligned} &HCN+OH\leftrightarrow CN+H_2O\\ &CN+O_2\leftrightarrow NO+CO\\ &CH_2+N_2\leftrightarrow HCN+NH\end{aligned} \tag{16}$$

For hydrocarbon fuels, the NO formation rate may be calculated by:

$$\frac{d[NO]}{dt}=f\;k'_{pr}[O_2]^{a}[N_2][FUEL]e^{-E'_a/RT} \tag{17}$$

where $f = 4.75 + 0.0819\,n - 23.2\,\varphi + 32\,\varphi^2 - 12.2\,\varphi^3$, $k'_{pr} = 6.4\times10^{6}(RT/p)^{a+1}$ and E'_a=303474.125 J/gmol. n is the number of carbon atoms per molecule for the hydrocarbon fuel, being equal to 1.149 for the present case, φ is the equivalence ratio (set here as φ=1) , a is the oxygen reaction order, which depends on the flame conditions. For oxygen molar fraction N_{O_2} greater than 4.1×10^{-3}, a is equal to one and above 0.03 it is zero, else

$$a=\begin{cases}-3.95-0.9\ln N_{O_2} & ;\quad 4.1\times10^{-3}\le N_{O_2}\le 1.11\times10^{-2}\\ -0.35-0.1\ln N_{O_2} & ;\quad 1.11\times10^{-2}\le N_{O_2}\le 0.03\end{cases} \tag{18}$$

Since the flow under analysis is turbulent, temperature and composition fluctuations are taken into account by considering probability density functions. In FLUENT NOx model, a joint-variable PDF in terms of a combination of a normalized temperature and species mass fraction is used to predict the NOx emission. No turbulent diffusion is considered in Eq. (10). The mean turbulent rate of production of NO, $\overline{S}_{NO}$, is given by:

$$\overline{S}_{NO}=\int\!\ldots\!\int S_{NO}(V_1,V_2,\ldots)\,P(V_1,V_2,\ldots)\,dV_1\,dV_2\ldots \tag{19}$$

where V_1, V_2, ….. are temperature and species concentrations, P is the probability density function, and $\overline{S}_{NO}$ is the instantaneous rate of production, given by eq. (11). This equation must be integrated at every node and at every iteration for the solution of Eq. (10).

RESULTS

The flow field inside the furnace was numerically obtained for the two types of oxidant. The solution was considered converged when the sum of the normalised residuals of all equations was less than 10^{-4} and the normalised enthalpy residual was less than 10^{-6}.

The mesh distribution was generated with the FLUENT auxiliary tool GAMBIT (Fluent, 2005) [9]. A grid test was performed, by doubling and by reducing in 50% the number of points in each direction. The overall agreement was very good, and the mesh was considered satisfactory for a maximum temperature difference smaller than 3%. After the grid test, an approximately uniform mesh of 134,400 control volumes, with $60 \times 40 \times 56$ elements in the x, y, and z directions, respectively, was selected. The smallest grid size was equal to 2 mm.

Initially pure oxygen was selected as oxidant. To accomplish the fusion of 16 tons of aluminum in one hour, a nominal thermal power equal to 1.2 MW per burner was specified, in order to represent both the energy necessary to melt the entire load of aluminum, and also the possible heat losses inherent in the process. Since the natural gas lower heating value h_{ci} is 44.8 MJ/kg, the fuel mass flow rate was set as 96.1 kg/h, which corresponds to an inlet fuel velocity of 126 m/s. The oxidant-fuel ratio was stoichiometrically defined, leading to an O_2 mass flow rate equal to 342 kg/h.

The O_2 mass fraction in the air is equal to 23%, therefore, for the second case, which employed air, the mass flow rate of air was defined as 1490 kg/h. However, for this case the amount of energy available for the aluminum fusion was significantly smaller than for the O_2 case, since it provided a heat transfer over the aluminum surface of 620 kW, and only 11 ton of melted aluminum could be obtained for the one hour period. To melt 16 tons, the duration of the process should be of least 1 hr and 25 minutes. This is probably due to the fact that an additional amount of energy is necessary to heat the nitrogen present in air, and also due to the large amount of nitrogen, a poor mixture of oxidant and fuel is obtained leading to a less efficient combustion.

To be able to compare the same process, a third case was analyzed, so that the same amount of melted aluminum in one hour could be obtained. The amount of fuel was increased so that a heat flux equal to 880 kW over the aluminum surface was obtained. The fuel mass flow rate was set as 148 kg/h (which corresponds to a 6.6 MW natural gas flame), and the air mass flow rate was set as 2258 kg/h.

Since the oxidant was injected through three openings, the total amount of oxidant mass flow rate was equally divided into each inlet.

To initiate the combustion process, a high temperature was specified as an initial guess to simulate the ignition.

Due to space limitations and since the qualitative behavior of both air cases are similar, only the comparison between this last case and the oxygen case will be presented.

Temperature and heat flux distribution

Figures 3 to 8 present a comparison of the temperature and heat flux distribution inside the furnace, with the two types of oxidant. The purpose of the comparison is to identify the influence of the type of oxidant in the flame shape, temperature distribution and heat flux distribution over the load.

As already mentioned, the cases selected to be presented produced the same total heat transfer rate of 880 kW over the aluminum surface. Figure 3 shows an isosurface of 1600K, while Fig. 4 illustrates the temperature distribution through a y-z plane passing by the burners (x=0.8 m). The temperature distributions at the refractory wall are shown in Fig. 5. To better analyze the influence of the oxidants, Figs. 6 and 7 show temperature profiles along selected lines inside the furnace.

The flame shape for both oxidants can be appreciated by examining the 1600K isosurfaces (Fig. 3). Both flames follow the direction of the inlet jets, away from the refractory walls and downward into the load's surface. The combustion starts near the entrance, where high values are obtained, and then the temperature level rapidly drops below 1600K. Figures 3a, 4a and 5a correspond to Case 1 (O_2) where a shorter and wider flame region can be seen, as well as higher temperatures. The maximum temperature inside the furnace is 3840 K. The air results are presented in Figs. 3b, 4b and 5b, where it can be seen that the flame is much longer and the temperatures are lower. For this case the maximum temperature inside the furnace is 1950 K.

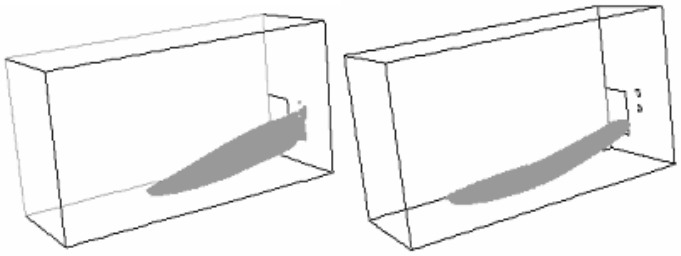

(a) O_2 (b) air

Fig. 3: Isosurfaces of temperature, T=1600 K.

By examining the temperature distribution on a plane that passes through the injectors (x = 0.80 m), Fig. 4, it can be seen for both cases, that the cold oxygen jet is over the natural gas jet, close to the inlet region. Due to the combustion, a substantial temperature rise can be observed, especially for the O_2 case. The temperature level inside the furnace is approximately the same for both oxidants (1400 K). However, it should be remembered that for Case 2, a larger amount of natural gas was injected to reach the same level of heat flux at the load.

While the air flame extends itself through the furnace, the O_2 flame is more intense and concentrated in the first half of the domain. This leads to a less uniform temperature distribution on the refractory walls (shown in Fig. 5) and could also compromise the uniformity of the heat flux on the aluminum surface (Fig. 8). In Fig. 5, the influence of the flame

at the refractory wall is clearly seen for the O_2 case, by the warm spots at the side wall (1446K). These warm spots can damage the refractory wall, increasing the cost of the project. Although warm spots were observed for the O_2 case, the average temperature at all the refractory walls are similar, around is 1360K. Also, since the flame is shorter, the maximum wall temperature is observed at the frontal plane (1708K). The wall temperature distribution for the air case (Fig 5b) is more uniform and the average wall temperature is 1407 K. The walls are cooler near the aluminum surface and warmer at the back wall, reaching a maximum of 1440 K.

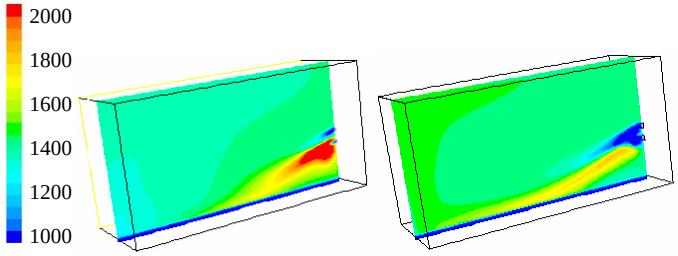

(a) O_2 (b) air

Fig. 4: Temperature (K) distribution. Plane y-z (x=0.8 m)

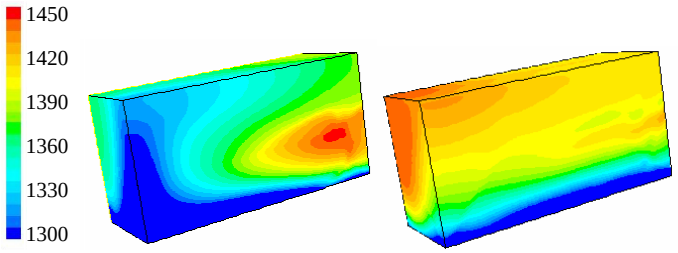

(a) O_2 (b) air

Fig. 5: Temperature (K) distribution on the refractory walls.

Figure 6 shows the temperature profile along the z coordinate for two lines inside the furnace. The first line (Fig. 6a) passes through the center of the burner (x = 0.80m and y = 0.65m), and another one (Fig. 6b) passes through the center of the oxidant injector (x = 0.80m and y = 0.85m). It can be seen that, as already mentioned, the temperature levels inside the furnace is around 1400K for both oxidant. Figure 7 presents the temperature profile along the x direction, at the height of the burner, at two z positions near the entrance. There is a small depression on the temperature level at y=0.65 m and z=0.90 m (Fig. 7b), for both cases. This is due to the fact that the inlets fuel/oxygen are cold, and only after both species are brought to contact, the combustion process starts. Since there is only oxygen in the lower entrance, it reduces the temperature of the warmer mixture that arrives from the upper burner. Due to the high amount of nitrogen in the air stream, it is more difficult for the oxygen to mix with the natural gas, therefore, the reaction starts farther away from the entrance and lower temperatures can be seen at z = 0.25 m. The peak of temperature for the O_2 case indicates that the reaction had already started at that location.

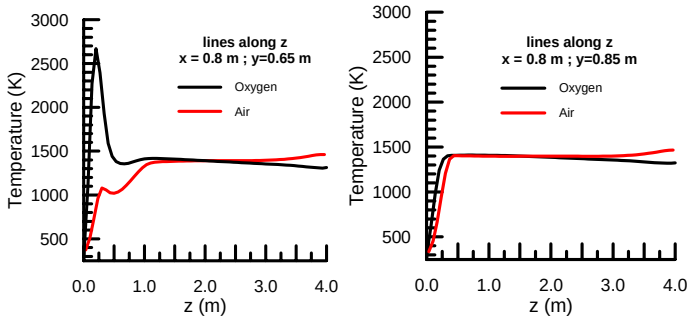

(a) x = 0.80 m; y = 0.65 m (b) x = 0.80 m; y = 0.85 m

Fig. 6: Temperature profiles along z inside the furnace.

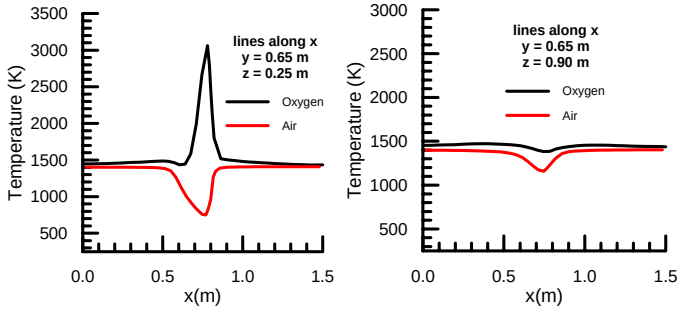

(a) y = 0.65 m; z = 0.25 m (b) y = 0.65 m; z = 0.90 m

Fig. 7: Temperature profiles along x inside the furnace.

The radiation heat flux on the aluminum surface is presented at Fig. 8. Due to the high temperature flame, the radiation heat flux is dominant. Large values of the radiation heat flux may be noted under the flame for both cases; however, since the O_2 flame was much more concentrated, a smaller high heat flux region can be seen near the entrance.

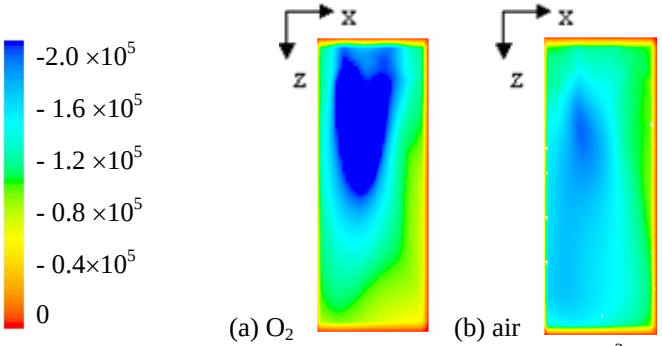

(a) O_2 (b) air

Fig. 8: Distribution of radiation heat flux (W/m^2)

Species distribution

The methane (CH_4) is the most abundant component in the natural gas, representing 77% of its mass composition. Therefore, the analysis of this species gives a good idea of how the fuel is consumed inside the furnace. The fuel reacts with the oxygen to form the products. The reactants distributions also

give a good idea of how the flame distributes itself along the furnace. The flame region is understood to be the region where the highest consumption of fuel occurs, followed by a large heat release and temperature raise. Comparison of the fuel and oxygen distributions for both cases are shown in Fig. 9, where iso-surfaces corresponding to 1% of mass fraction of CH_4 (red) and 5% mass fraction of O_2 (blue) are presented. The mass concentrations of both species are higher inside the respective isosurfaces. It can be seen the O_2 isosurface connected with the upper and lower burner. The CH_4 is injected only at the lower burner; therefore the CH_4 concentration is high, below the O_2 jet. It can be observed that the reaction occurs near the entrance, leading to low values of the reacting species in this region. It can be clearly seen that due to high amount of nitrogen present in the air, the O_2 distribution for this case is less concentrated, leading to a smaller 5% O_2 isosurface. Further, due to the presence of nitrogen, a bad contact between oxygen and natural gas may be noted.

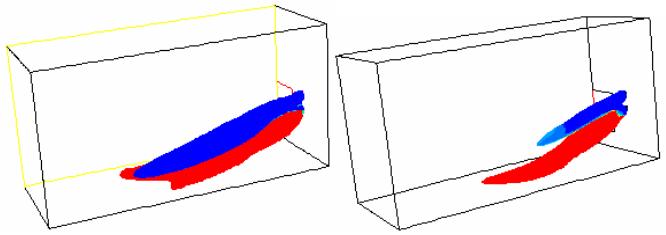

(a) O_2 (b) air

Fig. 9: Isosurfaces of 1% CH_4 (red) and 5% O_2 (blue)

The reaction of natural gas with oxygen is in two steps. Initially water and carbon monoxide are created, and then CO reacts with the oxygen creating carbon dioxide.

The carbon monoxide distribution inside the furnace can be seen at Fig. 10, at the plane that passes through the injectors (x = 0.80 m). The results for both air and O_2 cases are similar. It can be seen that CO is practically all consumed generating CO_2 for both oxidants. As expected the high CO concentration region coincides with the flame region, being longer for the air case. The second step reaction occurs in the lower part of the flame.

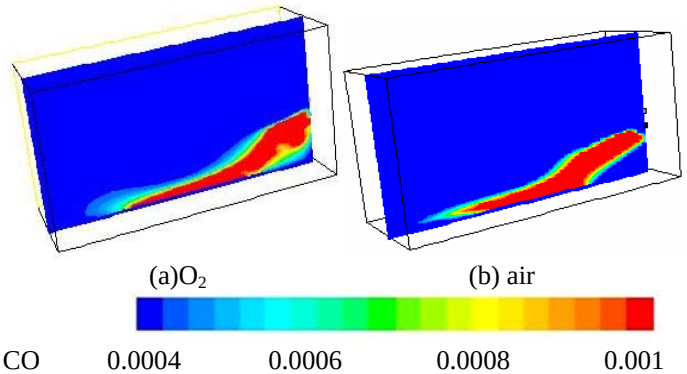

Fig. 10: Carbon Monoxide mass fraction inside the furnace. plane y-z (x=0.80 m)

Figure 11 shows the CO_2 distribution at several *x-y* planes along the *z* axial coordinate, for both oxidants. Since the products are still being formed, lower values may be observed in the flame region. A smaller amount of CO_2 may be noted for the air case, which is a positive aspect related with the selection of this oxidant. To better illustrate the amount of CO_2 that leaves the furnace, its distribution at the chimney is presented at Fig. 12. For both cases, the concentration of CO_2 at the chimney is approximately uniform. The air case has a mass fraction concentration equal to 27% of the O_2 case concentration.

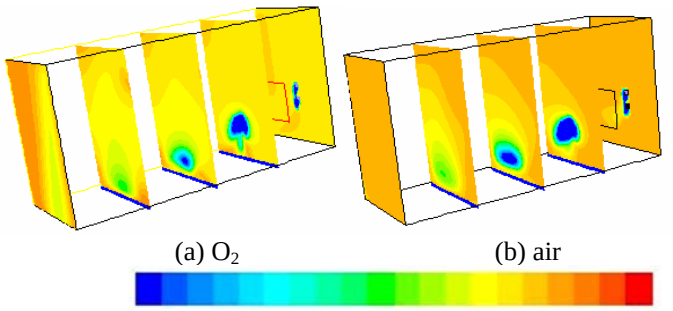

Fig. 11: Carbon Dioxide mass fraction inside the furnace. Planes x-y. z=0m, 1m, 2m, 3m and 4m.

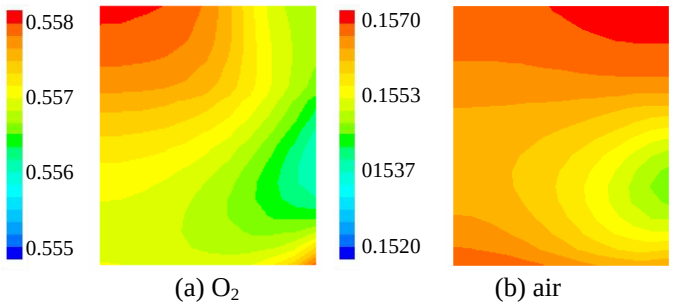

Fig. 12: Carbon Dioxide mass fraction at the chimney.

Although the amount of CO_2 is smaller for the air case, a second type of pollutant is formed, which is the NOx. Its mole fraction distribution is illustrated at Fig. 13 at the plane that passes through the injectors (x = 0.80 m) and at Fig. 14 at the chimney.

It can be seen that, as expected, the NOx distribution follows the same profile of all other species at the x=0.8 m. Further, its concentration is approximately uniform at the chimney, and its average value is equal to 4.25 ppm. The presence of NOx is the observed inconvenience in employing air instead of pure oxygen.

Figure 15 shows the water distribution over the aluminum surface. High water concentration is not desirable because an aluminum oxide layer can be formed as water reacts with the surface of the load, which increases the thermal resistance and compromises the quality of the product. It is interesting to

observe that the lowest water concentration is under the flame. Note however, that the water distribution is almost uniform in both cases. As with the CO_2 distribution, the air case produced smaller amount the water, which is also a desirable aspect, to avoid the aluminum oxidation.

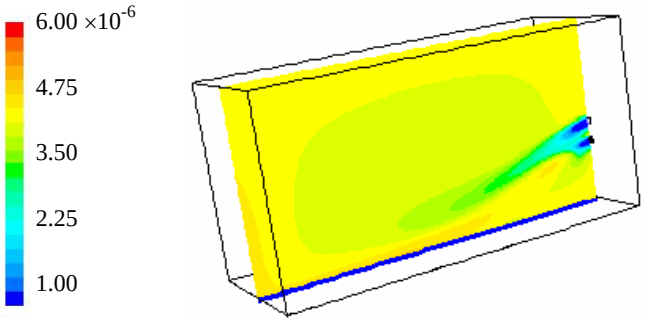

Fig. 13: NOx mole mass fraction at plane y-z, x=0.8 m.

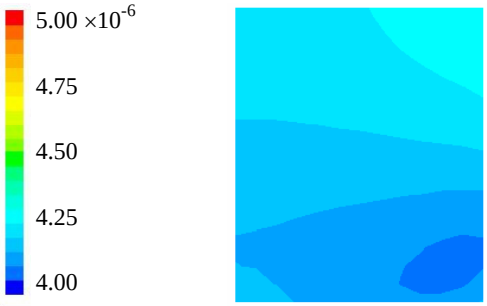

Fig. 14: NOx mole mass fraction at the chimney.

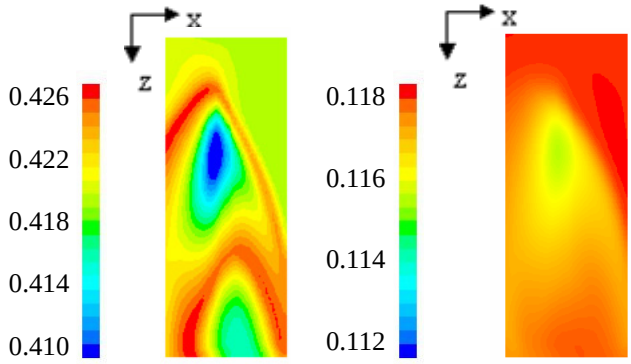

(a) O_2 (b) air

Fig. 15: Water mass fraction distribution on the aluminum surface.

CONCLUSION

The numerical simulation of the process inside an aluminum melting furnace proved to be a helpful tool, which can contribute to improve several aspects of industrial interest, for example, reduction of material costs on maintenance of the refractory walls, increase of the efficiency of the fusion process, assurance of the quality of the product by the investigation of the deposition of water on the aluminum surface, better positioning of the burner and oxygen injectors, etc.

The numerical simulation also allows the easy investigation of the influence of several variables on the process; however, the mathematical models that will be used must be carefully chosen to maximize reliability on the results, not bringing unreal physical situations representing the phenomena.

The choice of the type of oxidant used as energy source for the aluminum fusion can be crucial to achieve better efficiency on the process. It was seen that the option for pure oxygen or air as oxidant can significantly alter the combustion aspects inside the furnace, such as the formation of too long or too intense flames, leading to hot spots on the refractory walls and a non uniform heat flux distribution on the aluminum load.

Although a direct numerical comparison with experimental results was not performed due to lack of experimental data, the turbulence and combustion models employed here were used to predict the flow characteristics in the industrial aluminum remelting reverb furnace [4] with reasonable results. Further, the flow field was obtained with the same model in a cylindrical furnace [19] and good agreement with experimental data was obtained.

The present analysis showed that the selection of air as oxidant has several advantages in relation to the use of pure oxygen. The temperature level is lower, thus protecting the refractory walls, smaller products concentration were obtained at the chimney, and smaller water was found at the aluminum surface. Although a longer flame was obtained for with air, it did not present a significant impact at the refractory walls temperature. However, in order to produce the same amount of melted aluminum, a larger amount of air had to be specified, reducing the advantage of employing a cheaper oxidant. Further, a non-negligible amount of NOx was formed.

ACKNOWLEDGEMENT

The authors thank the Brazilian Research Council, CNPq, and Petrobras for the support during the development of this work.

REFERENCES

[1] Hill, SC, and Smoot, LD, 2000, “Modeling of nitrogen oxides formation and destruction in combustion systems”, Progress in Energy and Combustion Science, v 26, pp 417-558

[2] Frassoldati, A, Frigerio, S, Colombo, E, Inzoli, F, and Faravelli, T, 2005, ”Determination of NOx emissions from strong swirling confined flames with an integrated CFD-based procedure”, Chemical Engineering Science, v 60, pp 2851-2869.

[3] Nieckele, A.O., Naccache, M. F., Gomes, M. S. P., 2004, “Numerical Simulation of a Three Dimensional Aluminum Melting Furnace”, Journal of Energy Resources Technology, ASME, vol. 126, pp.72-81.

[4] Nieckele, A.O.; Naccache, M. F.; Gomes, M. S. P. and Kobayashi, W., 1999, "The influence of oxygen injection configuration in the performance of an aluminum melting furnace," Proceedings of 1999 ASME-IMECE, USA, Heat Transfer Division, **2**, pp. 405-412..

[5] Nieckele, A.O.; Naccache, M. F.; Gomes, M. S. P., Carneiro, J. N. E., and Silva, B. G., 2005, "Performance Of The Combustion Process Inside An Aluminum Melting Furnace With Natural Gas And Liquid Fuel," Proceedings of 2005 ASME-IMECE, USA, IMECE2005-79042.

[6] Brewster, B.S.; Webb, B.W.; McQuay; M.Q.,D'Agostini, M. and Baukal, C.E., 2001, "Combustion measurements and modelling in an oxygen-enriched aluminium-recycling furnace," Journal of the Institute of Energy, **74**, pp. 11-17.

[7] Mukhopadhyay, A.; Puri, I.K.; Zelepouga, S. and Rue, D.M., 2001, "Numerical simulation of methane-air nozzle burners for aluminum remelt furnaces," *Proceedings of 2001 ASME-IMECE*, USA, CD-ROM, HTD-24234.

[8] Nieckele, A.O.; Naccache, M.F.; Gomes, M. S. P.; Carneiro, J.N.E.; Serfaty, R., 2002, "Numerical simulation of natural gas combustion using a one step and a two step reaction", *Proceedings of 2002 ASME-IMECE*, November 11-16, New Orleans, LO, USA.

[9] Fluent User's Guide, v. 6.2, 2006, Fluent Inc., New Hampshire.

[10] Kuo, K.K., 1986. Principles of Combustion, John Wiley & Sons, New York.

[11] Launder, B.E. and Spalding, D.B., 1974. "The Numerical Computation of Turbulent Flows", Computer Methods in App. Mech. and Engineering, 3, p. 269-289.

[12] Patankar, S.V. and Spalding, D.B., 1967. Heat and Mass transfer in Boundary Layers, Morgan-Grampian, London.

[13] Smith, T.F., Shen, Z.F., and Friedman, J.N., 1982. "Evaluation of Coefficients for the Weighted Sum of Gray Gases Model", Transactions of the ASME - Journal of Heat Transfer, v. 104, p. 602-608.

[14] Magnussen, B. F. and Hjertager, B.H., 1976, On mathematical models of turbulent combustion with special emphasis on soot formation and combustion. In *16th Symp. (Int'l.) on Combustion*. The Combustion Institute.

[15] Tomeczek, J. and Gradón,B, 1997. "The Rate of Nitric Oxide Formation in Hydrocarbon Flames", Fourth International Conference on Technologies and Combustion for a Clean Environment, Lisbon , Portugal.

[16] Hanson, R. K. and Salimian, S. 1984, "Survey of Rate Constants in H/N/O Systems". In W. C. Gardiner, editor, *Combustion Chemistry*, page 361.

[17] Fenimore, C.P., 1971, "Formation of nitric oxide in premixed hydrocarbon flames", in 13th Int. Symp. on Combustion, p. 373, The Combustion Institute.

[18] Soete, G.G., 1975, "Overall reaction rates of NO and N2 formation from fuel nitrogen", 15th Symp. on Combustion, p. 1093-1102, The Combustion Institute.

[19] Nieckele, A.O.; Naccache, M.F., Gomes, M.S.P.; Carneiro, J.N.E.; Serfaty, R., 2001, "Models evaluations of combustion processes in a cylindrical furnace", *Procedings of 2001 ASME IMECE*, 2001, New York, NY, CD-ROM